

See discussions, stats, and author profiles for this publication at: <https://www.researchgate.net/publication/260868929>

# Enormous Plasmonic Enhancement and Suppressed Quenching of Luminescence from Nanoscale ZnO Films by Uniformly Dispersed Atomic-Layer-Deposited Platinum with Optimized Spacer Thickn...

ARTICLE *in* THE JOURNAL OF PHYSICAL CHEMISTRY C · NOVEMBER 2013

Impact Factor: 4.77 · DOI: 10.1021/jp406156n

---

CITATIONS

3

---

READS

29

## 5 AUTHORS, INCLUDING:



Chung-Ting Ko

National Taiwan University

9 PUBLICATIONS 24 CITATIONS

[SEE PROFILE](#)



Yin-Yi Han

National Taiwan University Hospital

30 PUBLICATIONS 265 CITATIONS

[SEE PROFILE](#)



Jay Shieh

National Taiwan University

55 PUBLICATIONS 468 CITATIONS

[SEE PROFILE](#)

# Enormous Plasmonic Enhancement and Suppressed Quenching of Luminescence from Nanoscale ZnO Films by Uniformly Dispersed Atomic-Layer-Deposited Platinum with Optimized Spacer Thickness

Chung-Ting Ko,<sup>†</sup> Yin-Yi Han,<sup>‡,§</sup> Ching-Hsiang Chen,<sup>||</sup> Jay Shieh,<sup>†</sup> and Miin-Jang Chen<sup>\*,†,⊥</sup>

<sup>†</sup>Department of Materials Science and Engineering, National Taiwan University, No. 1, Sec. 4, Roosevelt Road, Taipei 10617, Taiwan

<sup>‡</sup>Department of Traumatology, National Taiwan University Hospital, Taipei 10002, Taiwan

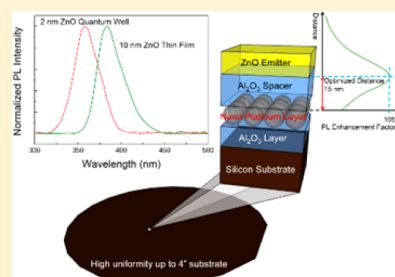
<sup>§</sup>Graduate Institute of Biomedical Electronic and Bioinformatic, National Taiwan University, Taipei 10617, Taiwan

<sup>||</sup>Protrustech Corporation Limited, 3F.-1, No. 293, Sec. 3, Dongmen Rd. East District, Tainan 70172, Taiwan

<sup>⊥</sup>National Nano Device Laboratories, Hsinchu 30078, Taiwan

## S Supporting Information

**ABSTRACT:** High-performance plasmonic ZnO/Al<sub>2</sub>O<sub>3</sub> spacer/nano-Pt/Al<sub>2</sub>O<sub>3</sub>/substrate multilayer structures were prepared by atomic layer deposition, in which the localized surface plasmons (LSP) were supported by the uniformly dispersed nanostructured Pt (nano-Pt) layer and a precise Al<sub>2</sub>O<sub>3</sub> spacer was introduced to suppress luminescence quenching. Over 100-fold enhancement of photoluminescence from the ZnO emitter, which facilitates the observation of significant quantum confinement effect in the nanoscale ZnO layer as thin as ~2 nm, was achieved. The giant plasmonic enhancement can be deduced from the optimized Al<sub>2</sub>O<sub>3</sub> spacer thickness, which leads to the reduced coupling with nonradiative high-order LSP modes as well as the overlap between the LSP resonance wavelength and the luminescence/absorbance spectra of the ZnO emitter. This plasmonic multilayer structure with high enhancement, accuracy, tunability, uniformity, and reproducibility can be further applied in sensitive bioassays/biosensing and efficient solid-state lighting.



## INTRODUCTION

Plasmonic enhancement of luminescence, or known as surface-enhanced luminescence (SEL) and metal-enhanced fluorescence, has been recognized as an effective method to enhance the intensity of luminescence from an emitter in the vicinity of metallic nanostructures.<sup>1–3</sup> Plasmon-enhanced luminescence has found a variety of applications such as labeling of biomolecules by fluorescence<sup>4–6</sup> and enhancement of electroluminescence efficiency of light-emitting diodes (LEDs).<sup>7–14</sup> Okamoto et al. demonstrated a 17-fold increase in the photoluminescence (PL) intensity from InGaN/GaN quantum wells when a nanostructured silver layer was deposited 10 nm above the quantum wells.<sup>15</sup> Kulakovich et al. used a layer-by-layer polyelectrolyte deposition technique to insert a well-defined spacer layer between the gold colloids and quantum dots, leading to the observation of a distance-dependent enhancement with the maximum PL increment by a factor of 5.<sup>16</sup> A nanopatterned Pt film onto ZnO film, as reported by Liu et al., was utilized to increase an order of magnitude of the near-band-edge emission from ZnO.<sup>17</sup> Recently, Lin et al. presented a 2.6-fold enhancement of ZnO PL intensity using a two-dimensional Al nanoparticles array.<sup>18</sup> The enhancement of luminescence can be attributed to the coupling with localized surface plasmons (LSPs) which are collective oscillations of free electrons within metallic nanostructures. The plasmonic

enhancement of light–matter interactions offers a new perspective to concentrate and manipulate light at the subwavelength scale, and accordingly enables a wide variety of applications including SEL and surface-enhanced Raman scattering (SERS).<sup>19–22</sup>

Both SEL and SERS induced by localized surface plasmon resonance (LSPR) can be understood in terms of the strong localization of electric field together with the concentration of photonic density of states (Purcell effect) around the metallic nanostructures.<sup>23,24</sup> However, significant difference between SEL and SERS has been reported in the literature.<sup>25–28</sup> SEL suffers from strong luminescence quenching as the light emitter is placed at a very short distance (a few nanometers) from the surface of plasmonic nanostructures, while SERS does not experience Raman quenching. Le Ru and Etchegoin deduced that the luminescence quenching originates from the coupling with nonradiative high-order LSP modes.<sup>29</sup> Sun and Khurgin have also concluded that the charge distributions on the metal surface of the high-order LSP modes result in zero dipole moments, thus being uncoupled to external radiation fields.<sup>30</sup> As a result, a precise nanoscale spacer layer with an optimal

Received: June 21, 2013

Revised: November 21, 2013

Published: November 25, 2013



thickness is needed to separate the emitter away from the metal surface, for reducing coupling with high-order LSP modes and thus preventing luminescence quenching to achieve significant enhancement of light emission.<sup>31</sup>

On the other hand, zinc oxide (ZnO) recently has been extensively investigated because of its direct and wide bandgap of 3.37 eV and a large exciton binding energy up to 60 meV.<sup>32</sup> The unique characteristics suggest that ZnO is a very promising material for next-generation ultraviolet (UV) LEDs and laser diodes. However, conventional plasmonic nanostructures made of gold (Au) and silver (Ag) can support tunable LSPR only in the visible and near-infrared spectra. In order to extend the activity of plasmonics into the UV wavelength, other plasmonic metals need to be explored. Platinum (Pt) has been considered as a possible candidate in UV plasmonics.<sup>33,34</sup> Furthermore, Pt nanostructures are of great interest for catalysis due to their high chemical potential and large surface area.<sup>35</sup> Therefore, Pt is quite an attractive material in UV plasmonics and LSPR-enhanced photocatalysis.<sup>36</sup>

Over the past decade, considerable advances in the fabrication of metallic nanostructures have enabled significant progress in plasmonics. The chemical synthesis of Au and Ag nanoparticles is the most popular technique for preparing plasmonic nanostructures.<sup>37–39</sup> Highly engineered nanofabrication techniques, including electron beam lithography and focused ion beam milling, are applied to accurately fabricate plasmonic nanostructures of various shapes and sizes.<sup>40,41</sup> Vacuum deposition techniques such as evaporation or sputtering are also extensively used to produce metallic nanoislands onto a substrate.<sup>42</sup> Nevertheless, the above nanofabrication techniques are usually limited by low throughput, poor uniformity, and low degree of reproducibility. Atomic layer deposition (ALD), which is capable of preparing nanoscale materials with monolayer accuracy, is another noteworthy technique for preparing high-quality plasmonic nanostructures.<sup>43–48</sup> In this study, ALD was used to fabricate ZnO/Al<sub>2</sub>O<sub>3</sub> spacer/nano-Pt/Al<sub>2</sub>O<sub>3</sub>/substrate multilayer structures, as shown in Figure 1, to explore the mechanism of plasmonic enhancement and to achieve the maximum PL enhancement in nanoscale ZnO ultrathin films. The plasmonic enhancement of light emission from ZnO was provided by

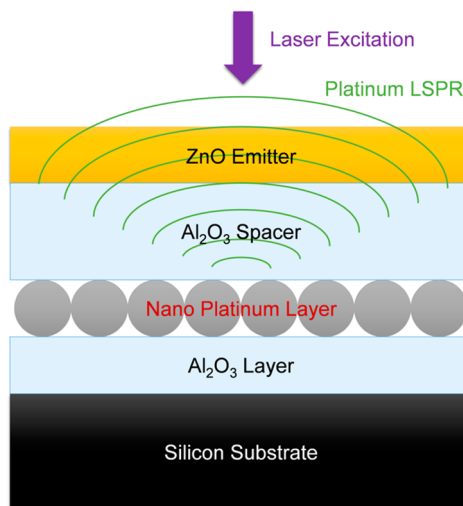


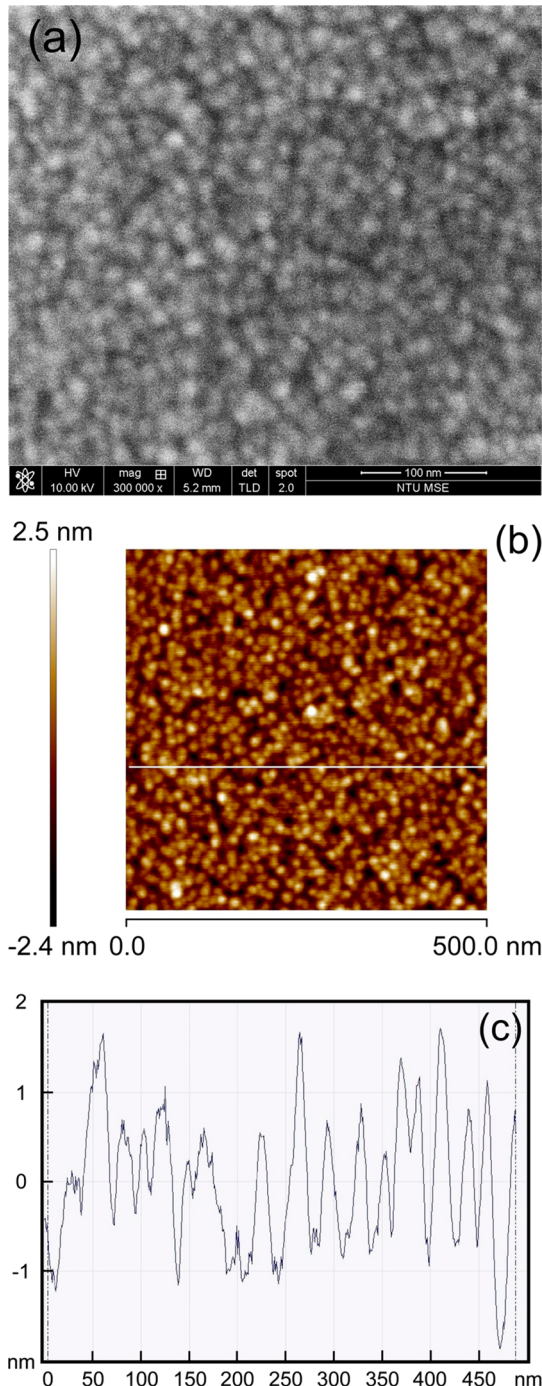
**Figure 1.** Schematic diagram of the plasmonic ZnO/Al<sub>2</sub>O<sub>3</sub> spacer/nano-Pt/Al<sub>2</sub>O<sub>3</sub>/substrate multilayer structure.

LSPR in the nanostructured Pt (nano-Pt) layer, and the luminescence quenching was suppressed by the Al<sub>2</sub>O<sub>3</sub> spacer introduced between the ZnO emitter and nano-Pt layer. The self-limiting and layer-by-layer growth of ALD offer a lot of advantages, including accurate thickness control, conformal step coverage, excellent uniformity, low defect density, good reproducibility, and low deposition temperatures. Thus, the thickness of the Al<sub>2</sub>O<sub>3</sub> spacer in the ZnO/Al<sub>2</sub>O<sub>3</sub> spacer/nano-Pt/Al<sub>2</sub>O<sub>3</sub>/substrate multilayer structures can be prepared “digitally” in a precise and well-controlled manner by ALD. In addition, the self-limiting growth and wide process window of ALD is a great benefit to the precise fabrication of the uniformly dispersed nanostructures in the nano-Pt layer with high reproducibility and uniformity over a large area. On the other hand, since the LSPR can be spectrally tuned by engineering the size, shape, and dielectric environment of the plasmonic nanostructures, intense research has been dedicated to the fabrication of metallic nanostructures with a variety of sizes and shapes.<sup>49,50</sup> The “digital” growth of the surrounding dielectrics around the plasmonic nanostructures by ALD offers an alternative way to accurately tailor the LSPR wavelength for spectral matching with the luminescence/absorbance of the light emitter.

Our previous study has demonstrated that the structures of nanoscale ultrathin films of a thickness only ~2 nm grown by ALD can be well characterized using the SERS technique.<sup>51</sup> In this paper, giant enhancement of light emission as large as 2 orders of magnitude from ZnO was accomplished by the ALD-grown nano-Pt layer and the optimized Al<sub>2</sub>O<sub>3</sub> spacer in the ZnO/Al<sub>2</sub>O<sub>3</sub> spacer/nano-Pt/Al<sub>2</sub>O<sub>3</sub>/substrate multilayer structures, with a high uniformity up to a 4 in. substrate. This plasmonic enhancement configuration leads to the observation of significant blue-shift in the PL spectrum from the nanoscale ZnO layer as thin as ~2 nm. The fundamental mechanism of plasmon-enhanced luminescence is elucidated in terms of the spacer dependence of the enhancement factor and the absorbance spectra of the ZnO/Al<sub>2</sub>O<sub>3</sub> spacer/nano-Pt/Al<sub>2</sub>O<sub>3</sub>/substrate multilayer structures.

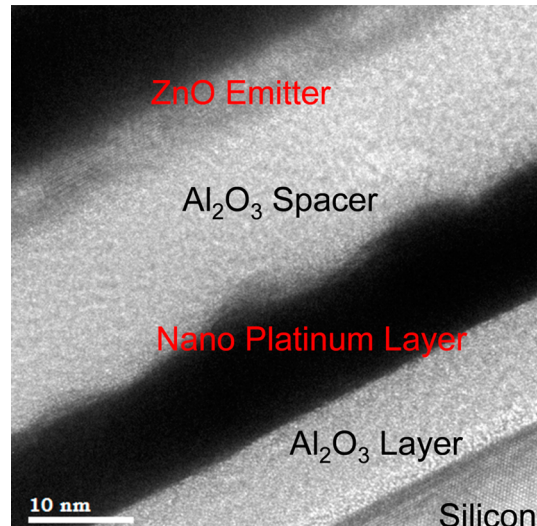
## RESULTS AND DISCUSSION

Figure 2 displays the surface morphologies of the nano-Pt layer characterized by scanning electron microscopy (SEM) and atomic force microscopy (AFM). While the Pt layer was macroscopically uniform, the SEM image in Figure 2a reveals the presence of Pt nanoparticels, indicating the nanoscale Pt layer deposited on Al<sub>2</sub>O<sub>3</sub> aggregates to nanoparticles for the reduction of the surface energy due to the great difference in the surface energy between Al<sub>2</sub>O<sub>3</sub> and Pt.<sup>52</sup> The nano-Pt layer prepared by ALD consists of uniformly dispersed Pt nanoparticles about 10 nm in diameter, which is at the resolution limit of SEM. The AFM image of the nano-Pt layer with a scanning area of 500 × 500 nm<sup>2</sup> is presented in Figure 2b. The nanoparticles with a uniform distribution of particle size were observed in the nano-Pt layer, which is consistent with the SEM image shown in Figure 2a. The line-scan profile of the AFM image, as shown in Figure 2c, reveals that the corrugation in topography of the nano-Pt layer is about ±1 nm and the Pt nanoparticles are uniformly distributed in the lateral dimension. It should be noted that the distortion in quantitative characterization of spatial features can be expected since the spacing and size of the Pt nanoparticles are smaller than or close to the typical diameter of the AFM tip. The observation of Pt nanoparticles grown by ALD shown in Figure 2 is consistent



**Figure 2.** (a) SEM and (b) AFM images display the surface morphologies of the nano-Pt layer. The line-scan analysis of the AFM image is shown in (c).

with those reported by Novak et al.,<sup>53</sup> Altonen et al.,<sup>54</sup> and Baker et al.,<sup>52</sup> indicating that the growth of Pt at the initial stage of ALD follows the Volmer–Weber mode. The cross-sectional high-resolution TEM (HRTEM) image of sample Z-5 is shown in Figure 3. It can be seen that the thickness of the  $\text{Al}_2\text{O}_3$ , nano-Pt,  $\text{Al}_2\text{O}_3$  spacer, and  $\text{ZnO}$  emitter is 10.2, 10.6, 15.1, and 5.4 nm, respectively. The thickness of each layer well coincides with the estimation of applied ALD cycles, manifesting the excellent thickness controllability of ALD. The roughness between the nano-Pt layer and the  $\text{Al}_2\text{O}_3$  spacer suggests that



**Figure 3.** Cross-sectional HRTEM image of the sample Z-5.

the Pt layer was constructed from Pt nanoparticles bundled together, in agreement with the SEM and AFM observations.

Figure 4a shows the room-temperature PL spectra of the samples S-0, S-5, ..., and S-45, in which the thickness of the  $\text{Al}_2\text{O}_3$  spacer in the  $\text{ZnO}/\text{Al}_2\text{O}_3$  spacer/nano-Pt/ $\text{Al}_2\text{O}_3$ /substrate multilayer structure ranges from 0 to 45 nm, with an interval of 5 nm. It is seen that significant UV luminescence at  $\sim 380$  nm was observed from each sample, which can be ascribed to the near-band-edge emission from excitons in the

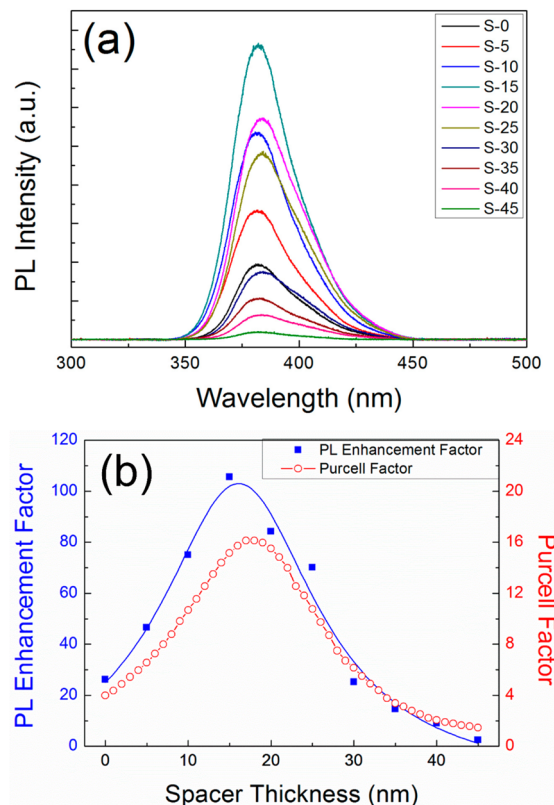


**Figure 4.** (a) Room-temperature PL spectra of the samples S-0, S-5, ..., and S-45. (b) Measured PL enhancement factor and simulated Purcell factor as a function of the  $\text{Al}_2\text{O}_3$  spacer thickness, of the  $\text{ZnO}/\text{Al}_2\text{O}_3$  spacer/nano-Pt/ $\text{Al}_2\text{O}_3$ /substrate multilayer structures.

10 nm ZnO layer. The variation of PL intensity with the  $\text{Al}_2\text{O}_3$  spacer thickness suggests the competition between the plasmonic enhancement and luminescence quenching. In order to calculate the PL enhancement factor, the reference samples with the multilayer structures similar to the samples S-0, S-5, ..., and S-45 were also prepared. All the thicknesses of each layer and the process conditions of the samples S-0, S-5, ..., and S-45 are the same as those of each corresponding reference sample, except that the nano-Pt layer was not grown in the reference samples. The plasmonic enhancement factor of PL was obtained by normalization of the total integrated PL intensity of the samples S-0, S-5, ..., and S-45 to that of each corresponding reference sample. Figure 4b shows the measured PL enhancement factor and the simulated Purcell factor as a function of the  $\text{Al}_2\text{O}_3$  spacer thickness. The Purcell factor of the  $\text{ZnO}/\text{Al}_2\text{O}_3/\text{nano-Pt}/\text{Al}_2\text{O}_3/\text{substrate}$  multilayer structures was calculated by the finite difference time domain (FDTD Solutions 8.6, Lumerical Solutions Inc.) method. In the simulation, a dipole source radiating normal to the surface at  $\lambda = 380$  nm was placed within the nanoscale ZnO layer. The dielectric function of platinum was described by the Drude–Lorentz model, and the morphology of the nano-Pt layer was depicted as randomly and uniformly dispersed nanoparticles. The simulation was carried out with the perfectly matched layers in the vertical direction and the periodic boundary condition in the horizontal direction to truncate the computational domain. With an increase of the  $\text{Al}_2\text{O}_3$  spacer thickness from 0 to 45 nm, the measured PL enhancement factor increases and reaches a maximum as the spacer thickness equals to 15 nm (sample S-15). Then the PL enhancement drops rapidly and approaches to a low value close to 1 at the spacer thickness of 45 nm, at which the PL intensity of sample S-45 approximates to that of its reference sample without the enhancement from the nano-Pt layer. A huge plasmonic enhancement of PL as large as  $\sim 105$  from the ZnO emitter was achieved in the multilayer structure with the ALD-grown nano-Pt layer and optimized  $\text{Al}_2\text{O}_3$  spacer thickness of 15 nm. It can be also seen from Figure 4b that the simulated Purcell factor follows the similar trend as the measured PL enhancement factor, except the difference between their magnitudes. Thus, the simulated Purcell factor provides a supportive evidence of the plasmonic enhancement in the  $\text{ZnO}/\text{Al}_2\text{O}_3/\text{nano-Pt}/\text{Al}_2\text{O}_3/\text{substrate}$  multilayer structures. The difference in the magnitudes of the measured PL enhancement factor and the simulated Purcell factor can be ascribed to the absorption enhancement in the plasmon-enhanced PL process, which is not included in the simulation of Purcell factor.

In order to elucidate the mechanism of plasmonic PL enhancement in terms of LSPR, the absorbance spectra of the  $\text{ZnO}/\text{Al}_2\text{O}_3/\text{nano-Pt}/\text{Al}_2\text{O}_3/\text{substrate}$  multilayer structures were examined. Figure 5a shows the absorbance spectra of the samples S-0, S-5, ..., and S-45. The spectral peak around 380 nm in all the samples originates from the near-band-edge absorbance of the ZnO layer. Another absorbance peak of each sample, as indicated by the arrow, can be attributed to the LSPR in the nano-Pt layer. Generally, the Pt nanostructures with features size less than 100 nm exhibit LSPR in the deep-UV region.<sup>33,34</sup> The absorbance spectra in Figure 5a were fitted with multiple Gaussian functions in the frequency domain, and accordingly, the maximum absorbance wavelength ( $\lambda_{\max}$ ) associated with LSPR in the nano-Pt layer can be extracted. It can be seen in Figure 5a that LSPR  $\lambda_{\max}$  is 244 nm for the S-0 sample, in which the  $\text{Al}_2\text{O}_3$  spacer thickness is zero and the

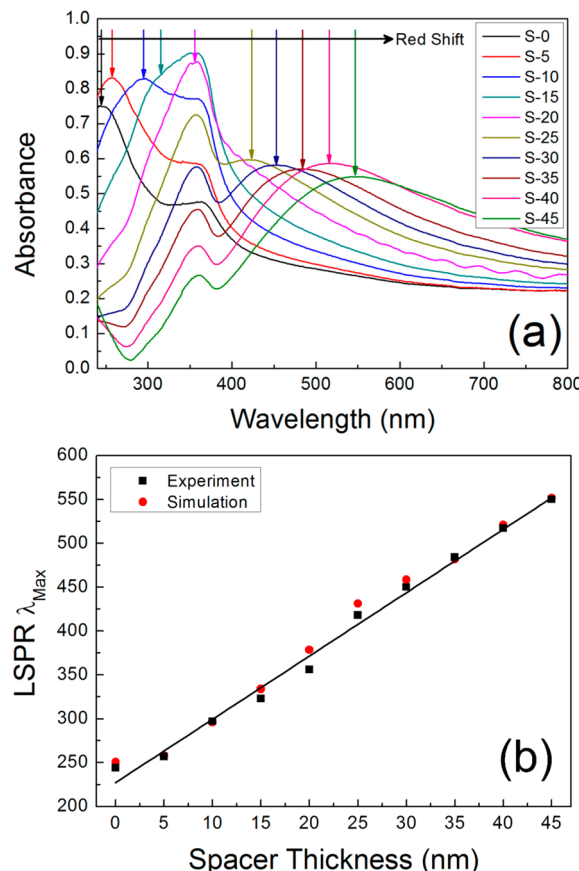


**Figure 5.** (a) Absorbance spectra of the samples S-0, S-5, ..., and S-45. (b) Measured and simulated LSPR  $\lambda_{\max}$  as a function of the  $\text{Al}_2\text{O}_3$  spacer thickness.

ZnO emitter directly contacts with the nano-Pt layer. Then LSPR  $\lambda_{\max}$  gradually red-shifts from the deep-UV region toward the visible spectrum with an increase of the  $\text{Al}_2\text{O}_3$  spacer thickness. A plot of the measured and simulated LSPR  $\lambda_{\max}$  versus the  $\text{Al}_2\text{O}_3$  spacer thickness is shown in Figure 5b, both revealing a linear red-shift and broad spectral tuning range of LSPR  $\lambda_{\max}$  from 244 nm (sample S-0) to 547 nm (sample S-45) with the increasing thickness of the  $\text{Al}_2\text{O}_3$  spacer. The electrodynamic simulation of the LSPR  $\lambda_{\max}$  associated with the nano-Pt layer in the  $\text{ZnO}/\text{Al}_2\text{O}_3/\text{nano-Pt}/\text{Al}_2\text{O}_3/\text{substrate}$  multilayer structures was also performed by the FDTD method. A total-field/scattered-field formulation was used to introduce the incident plane wave. The dielectric function of Pt, morphology of the nano-Pt layer, and boundary condition of the computational domain are the same as those used in the simulation of the Purcell factor as mentioned above. The excellent agreement between the simulated and experimental results gives support to the spectral shifting in the LSPR  $\lambda_{\max}$  by engineering the dielectric environment around the plasmonic nanostructures, which is also consistent with the wavelength tuning of LSPR using dielectric layers as those reported in refs 50, 55, and 56. Since the effective refractive index around the nano-Pt layer increases with the  $\text{Al}_2\text{O}_3$  spacer thickness due to the higher refractive index of  $\text{Al}_2\text{O}_3$  than the air, such a significant red-shift in LSPR  $\lambda_{\max}$  can be deduced from the increase in effective refractive index of environmental dielectric around the nano-Pt layer. The result shown in Figure 5 clearly demonstrates that the LSPR wavelength can be precisely tuned using ALD by the “digital” growth of the

surrounding dielectrics around plasmonic nanostructures. It should be noted that the LSPR peaks of the samples S-15 and S-20 overlap with the near-band-edge absorbance of the ZnO emitter around 380 nm. As seen from Figure 4, maximum PL enhancement also takes place in the plasmonic multilayer structure with the Al<sub>2</sub>O<sub>3</sub> spacer thickness of 15 and 20 nm, clearly indicating that the coincidence of the LSPR  $\lambda_{\max}$  with the absorbance of the light emitter is critical to the enormous plasmonic enhancement of luminescence.

The mechanism of plasmon-enhanced PL can be clarified in terms of the energy flow diagram as shown in Figure 6, together

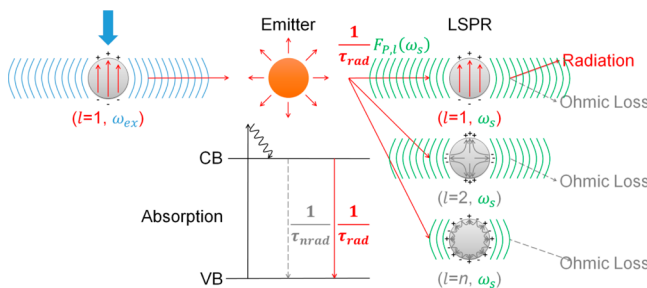


**Figure 6.** Illustration of plasmon-enhanced luminescence from an emitter in proximity to a metal nanoparticle based on the effective volume theory.

with the effective volume theory proposed by Maier<sup>57</sup> and developed analytically by Sun and co-workers.<sup>30,31</sup> First, the dipole ( $l = 1$ ) LSP mode in plasmonic nanostructures is excited by the incident photons of frequency  $\omega_{\text{ex}}$ . Since the electric field in the local area near plasmonic nanostructures is significantly enhanced by the dipole LSP mode, the absorption of the light emitter at a small distance  $d$  away from the surface of plasmonic nanostructures is enhanced according to the Fermi's golden rule. Following the absorption, the excited electrons experience a series of rapid intraband relaxation processes, reaching the conduction band edge after several picoseconds, and then remain there for a few nanoseconds. If the emitter is not in proximity to plasmonic nanostructures, the electrons subsequently decay to the valence band through the interband transitions characterized by the radiative and the nonradiative decay rates  $\tau_{\text{rad}}^{-1}$  and  $\tau_{\text{nrad}}^{-1}$ , respectively. In the presence of metallic nanostructures adjacent to the emitter, an additional path is created for the electrons at the conduction band edge to relax their energy at the luminescence frequency  $\omega_s$  into the LSP modes in plasmonic nanostructures. The coupling rate into the  $l$ th LSP mode is given by  $F_{p,l}\tau_{\text{rad}}^{-1}$ , where  $F_{p,l}$  is the Purcell factor of the  $l$ th LSP mode.<sup>31</sup> As compared with the original radiative decay rate  $\tau_{\text{rad}}^{-1}$ , the coupling between the emitter and the  $l$ th LSP mode is enhanced by the Purcell factor  $F_{p,l}$  as a result of the enhanced electric field at the frequency  $\omega_s$  in the vicinity of plasmonic nanostructures. The Purcell factor  $F_{p,l}$  can be expressed as the ratio of the density of states of the  $l$ th LSP mode to that of the free-space photon mode. Since the density of plasmonic states exhibits a peak at plasmonic resonance, the Purcell factor  $F_{p,l}$  has a maximum at the LSPR wavelength. The confinement of electric field near the surface of plasmonic nanostructures can be characterized by the effective mode volume,<sup>31,57</sup> which decreases with the increase of the mode index  $l$ .<sup>30,31</sup> Thus, the energy of electric field is increasingly concentrated in a smaller region very close to plasmonic nanostructures for the high-order LSP modes. The smaller effective volumes indicate that the coupling between the

emitter and high-order LSP modes is rather efficient with a decrease of the separation  $d$ . However, the charge distributions of the high-order ( $l > 1$ ) LSP modes results in zero dipole moments, and so the high-order ( $l > 1$ ) LSP modes are uncoupled to free-space photons.<sup>30</sup> Thus, the energy transferred to the high-order ( $l > 1$ ) LSP modes merely dissipates as the metal (ohmic) loss and contributes nothing to light emission. On the other hand, the surface charge distribution of the fundamental ( $l = 1$ ) LSP mode yields a nonzero dipole moment, which is capable of interacting with free-space photons. Therefore, only the dipole ( $l = 1$ ) LSP mode can act as the additional path for radiative decay and thus contribute to the plasmonic enhancement of luminescence. Since the overall plasmonic enhancement process comprises the absorption at  $\omega_{\text{ex}}$  and the luminescence at  $\omega_s$ , the total enhancement of light emission is the product of the absorption and luminescence enhancement. The coupling into all the high-order ( $l > 1$ ) LSP modes results in luminescence quenching as the emitter is located in close vicinity to the plasmonic nanostructures.<sup>31</sup> Therefore, an appropriate spacing between the emitter and plasmonic nanostructures is necessary for significant suppressing the luminescence quenching associated with the high-order modes as well as sufficient coupling into the dipole LSP mode.

According to the above discussions, the PL enhancement factor as a function of the Al<sub>2</sub>O<sub>3</sub> spacer thickness shown in Figure 4b can be explained as follows. As the spacer thickness increases from 0 to 15 nm, the coupling into the high-order ( $l > 1$ ) LSP modes is suppressed and the LSPR  $\lambda_{\max}$  of the nano-Pt layer shifts toward the near-band-edge luminescence/absorbance spectra of the ZnO emitter as well. As a result, a giant plasmonic PL enhancement up to  $\sim 105$ -fold was achieved. The decrease of the PL enhancement factor with the spacer thickness from 15 to 45 nm can be deduced from the rapid decrease of electric field with the distance away from the nano-Pt layer, together with off-resonance between the light emitter and the LSP modes. The optimized Al<sub>2</sub>O<sub>3</sub> spacer thickness corresponding to the maximum PL enhancement factor is 15 nm. Nevertheless, Figure 5a shows that the LSPR peak of the nano-Pt layer coincides with the near-band-edge ZnO absorbance in the multilayer structure with a spacer thickness of 20 nm. The slight difference might result from the enhanced coupling into the dipole LSP mode due to the higher electric field at a smaller spacing of 15 nm.

With the huge plasmonic enhancement of PL due to the ALD-grown nano-Pt layer and the optimized Al<sub>2</sub>O<sub>3</sub> spacer thickness of 15 nm, the ZnO/Al<sub>2</sub>O<sub>3</sub> spacer/nano-Pt/Al<sub>2</sub>O<sub>3</sub>/substrate multilayer structure was used to probe the PL from the ultrathin ZnO layer with the feature size approaching the quantum region. Figure 7a shows the room-temperature PL spectra of the samples Z-2, Z-3, ..., and Z-10, in which the thickness of the ZnO emitter ranges from 2 to 10 nm, with an interval of 1 nm. The ultrathin ZnO layers exhibit a dominant near-band-edge luminescence, with a significant blue-shift of the PL spectral peak from 380 to 358 nm as the film thickness decreases from 10 to 2 nm, as shown in Figure 7b. The blue-shift in the PL spectrum can be ascribed to the quantum confinement effect in the nanoscale ZnO ultrathin film, which can be described simply using an infinite quantum well model.<sup>58</sup>

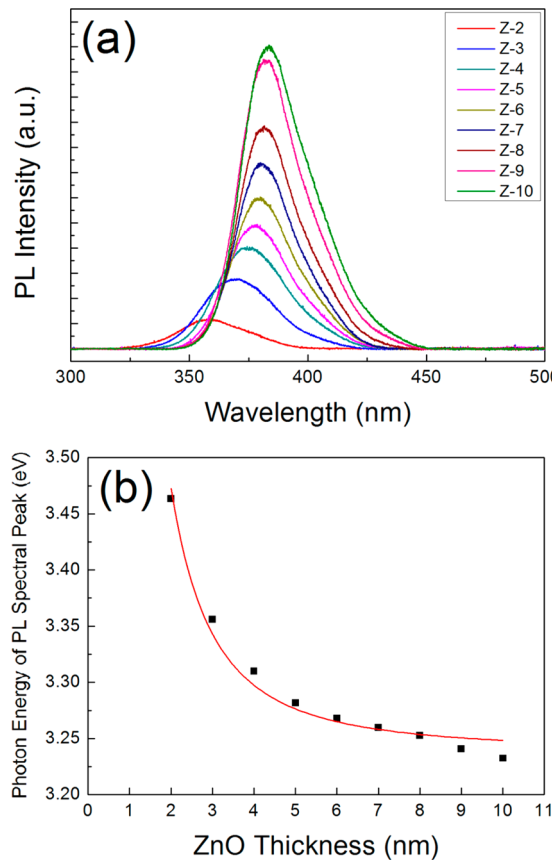


**Figure 7.** (a) Room-temperature PL spectra of the samples Z-2, Z-3, ..., and Z-10. (b) Dependence of the PL spectral peak on the thickness of the nanoscale ZnO ultrathin layer.

$$\Delta E = \frac{\pi^2 \hbar^2}{2L^2} \left( \frac{1}{m_e^*} + \frac{1}{m_h^*} \right) = \frac{\pi^2 \hbar^2}{2L^2} \frac{1}{\mu} \quad (1)$$

where  $\Delta E$  is the energy shift of the PL spectral peak,  $\hbar$  and  $L$  are reduced Plank's constant and the thickness of the ZnO quantum well, respectively,  $m_e^*$  and  $m_h^*$  are the electron and hole effective masses, respectively, and  $\mu$  is the reduced mass of electron–hole pair. Figure 7b shows that the blue-shift in the PL spectrum with the ZnO thickness can be well fitted by eq 1, with a slight departure of the reduced mass  $\mu = 0.4m_0$  from those reported for crystalline bulk ZnO ( $\mu = 0.21m_0$ ).<sup>59–62</sup> This difference can be deduced from the poor crystallinity of the ZnO layer as shown in the HRTEM image (Figure 3), or the assumption of infinite potential barrier used in eq 1. It can be expected that the poor crystallinity of the nanoscale ZnO layer prepared by ALD at a low temperature (180 °C) results in a low carrier mobility, leading to a higher effective mass.<sup>63</sup> On the other hand, in the quantum wells with finite barriers, the electron wave functions spread out into the barriers, thereby reducing the quantum confinement effect and giving rise to the less blue shift of the energy level as compared with the infinite quantum well. Therefore, when the infinite quantum well model was applied to fit the blue-shift in the PL spectrum shown in Figure 7b, the reduced quantum confinement effect due to the finite potential barrier of Al<sub>2</sub>O<sub>3</sub> resulted in a higher reduced mass. It may be noted that the measurement of PL spectrum from the ultrathin ZnO layer of only ~2 nm in thickness is not possible without plasmonic enhancement from the nano-Pt layer. Hence, the observation of PL from the ZnO

quantum well as thin as ~2 nm actually reveals that the plasmonic multilayer structures prepared by ALD is a powerful characterization method, for probing the weak light emission from the nanoscale materials approaching the quantum confinement limit.

The uniformity of the ZnO/Al<sub>2</sub>O<sub>3</sub> spacer/nano-Pt/Al<sub>2</sub>O<sub>3</sub>/substrate multilayer structure over a 4 in. substrate is shown in the Supporting Information. The PL intensity from the ZnO emitter in the plasmonic multilayer structure exhibits a small fluctuation of only ±1.11% across the entire area. The variations of pseudorefractive index and extinction coefficient of the multilayer structure are ±2.29%, and ±1.48% over the substrate, respectively. Since the pseudorefractive index and extinction coefficient, as well as the PL intensity, are sensitive to the thickness and microstructure of each layer, the result clearly manifests the high uniformity of the plasmonic nanostructures prepared by the ALD technique. This high uniformity can be attributed to the self-limiting growth, leading to insensitivity to the inhomogeneity of substrate temperature and precursor distribution in the ALD process. Since the thin films required in the plasmonic applications are usually only about a few tens of nanometers in thickness, the high degree of uniformity over a large area may compensate for the low deposition rate of ALD, which suggests the high throughput of the plasmonic substrates fabricated by ALD as compared with other nanofabrication approaches. In addition, it has been demonstrated that the ultrathin ALD coating can effectively protect the plasmonic nanostructures against harmful environments due to the dense and pinhole-free structure, conformal coverage, and low deposition temperatures of the ALD films.<sup>64–66</sup> Thus, the ALD technique offers an excellent capability of fabricating, decorating, and tuning the plasmonic nanostructures and properties, with inherent high precision, uniformity, and reproducibility over a large area. The distinguished characteristics of the uniform multilayer structures prepared by ALD can find applications in plasmonic enhancement of the light emission from quantum wells and the fluorescence from the biomolecules attached upon the spacer.

## CONCLUSION

In summary, high-performance plasmonic nanostructures consisting of ZnO/Al<sub>2</sub>O<sub>3</sub> spacer/nano-Pt/Al<sub>2</sub>O<sub>3</sub>/substrate multilayers with high precision, tunability, uniformity, and reproducibility were demonstrated. The plasmonic enhancement was contributed by the nano-Pt layer with a uniform distribution of nanoparticle size grown by ALD. Luminescence quenching was suppressed, due to the reduced coupling with the nonradiative high-order LSP modes, by a precise Al<sub>2</sub>O<sub>3</sub> spacer prepared by the digital growth of ALD. The LSPR of the nano-Pt layer can be spectrally tuned to overlap with the ZnO luminescence/absorbance spectra by accurate control of the surrounding dielectrics around the nano-Pt layer. The plasmonic multilayer structure, with a high spatial uniformity up to a 4 in. substrate, leads to an over-100 fold enhancement of light emission from the ZnO emitter and the observation of significant blue-shift in the PL spectrum from 380 to 358 nm from the ZnO quantum well as thin as ~2 nm. This remarkable configuration of plasmon-enhanced luminescence can be considered as a stable and potential platform to enhance the luminescence from solid-state quantum wells and the fluorescence from biomolecules in the near future.

## EXPERIMENTAL SECTION

Figure 1 shows the schematic diagram of the ZnO/Al<sub>2</sub>O<sub>3</sub> spacer/nano-Pt/Al<sub>2</sub>O<sub>3</sub>/substrate multilayer structure. All of the layers upon the Si substrate were prepared via the thermal ALD system (Savannah 100, Cambridge Nanotech). The ZnO and Al<sub>2</sub>O<sub>3</sub> layers were deposited at 200 and 180 °C, respectively, using diethylzinc [DEZn, Zn(C<sub>2</sub>H<sub>5</sub>)<sub>2</sub>], trimethylaluminum [TMA, Al(CH<sub>3</sub>)<sub>3</sub>], and H<sub>2</sub>O vapor as the precursors. Trimethyl(methylcyclopentadienyl)platinum(IV) [(MeCp)PtMe<sub>3</sub>] and oxygen were used to grow the nano-Pt layer at 270 °C. First, a 10 nm thick Al<sub>2</sub>O<sub>3</sub> thin film was deposited on the Si substrate. Next, 100 ALD cycles were applied to prepare the nano-Pt layer on the Al<sub>2</sub>O<sub>3</sub> thin film. The Pt growth starts with the discrete nanoclusters during the first a few ALD cycles.<sup>52,54,67,68</sup> If the Pt layer is not thick enough, the Pt nanoclusters would not coalesce together to form a continuous film, leading to the formation of a nanostructured Pt layer. Afterward, an Al<sub>2</sub>O<sub>3</sub> spacer layer was deposited upon the nano-Pt layer. Thus, the nano-Pt layer was wrapped by the Al<sub>2</sub>O<sub>3</sub> spacer and the underlying Al<sub>2</sub>O<sub>3</sub> thin film in this multilayer structure, so as to make the dielectric environment around the nano-Pt layer less complicated. Finally, a nanoscale ZnO layer was grown on the Al<sub>2</sub>O<sub>3</sub> spacer. The Al<sub>2</sub>O<sub>3</sub> spacer introduced between the ZnO light emitter and the plasmonic nano-Pt layer was aimed to suppress luminescence quenching. The thickness of Al<sub>2</sub>O<sub>3</sub> spacer and the morphology of nano-Pt layer can be precisely and “digitally” controlled by the number of introduced ALD cycles in a layer-by-layer growth mode. For the sake of convenience, the plasmonic multilayer structures were named as S-X according to the Al<sub>2</sub>O<sub>3</sub> spacer thickness of X nm, in which the thickness of the ZnO emitter is 10 nm. Another group of samples were designated as Z-Y, where Y represents the thickness of the ZnO emitter layer (in nm), accomplished with a 15 nm thick Al<sub>2</sub>O<sub>3</sub> spacer layer.

The ZnO/Al<sub>2</sub>O<sub>3</sub> spacer/nano-Pt/Al<sub>2</sub>O<sub>3</sub>/substrate multilayer structures and the thickness of each layer were characterized by high-resolution transmission electron microscopy (HRTEM, JEOL, JEM-2100F). The sample for cross-sectional TEM measurement was prepared by focused ion beam (FIB, FEI NOVA-200 NanoLab Compatible). The surface morphology of nano-Pt layer was examined by scanning electron microscopy (SEM, FEI NOVA NanoSEM 450) and atomic force microscopy (AFM, Nanonics MV4000 kit). The pseudo-dielectric function of the multilayer structure was extracted by ellipsometer at  $\lambda = 633$  nm (Gaertner Scientific, model L116SF300). The plasmonic multilayer structures were excited by a pulsed Q-switched diode-pumped solid-state laser (Advanced Optowave Corporation,  $\lambda = 266$  nm, repetition rate = 3 kHz) in order to obtain the PL spectra, which were collected by the micro-PL (ProMaker) system mounted with one TE cooled Andor-iDus CCD of 1024 × 256 pixels as integrated by Protrustech Corporation Limited. An ultraviolet-visible spectrophotometer (JASCO Ubest V-570) was used to probe the absorbance spectra of the plasmonic multilayer structures.

## ASSOCIATED CONTENT

### Supporting Information

Pseudorefractive index and extinction coefficient, as well as the PL spectrum and intensity, from a 9-point map of the ZnO/Al<sub>2</sub>O<sub>3</sub> spacer/nano-Pt/Al<sub>2</sub>O<sub>3</sub>/substrate multilayer structure on

a 4-in. substrate. This material is available free of charge via the Internet at <http://pubs.acs.org>.

## AUTHOR INFORMATION

### Corresponding Author

\*E-mail: mjchen@ntu.edu.tw. Tel: +886-2-3366-5301.

### Notes

The authors declare no competing financial interest.

## ACKNOWLEDGMENTS

This work is partially supported by the National Science Council of Taiwan, Republic of China (NSC 102-2325-B-002-013, 102-2120-M-002-003, 102-2628-M-001-008, 102-ET-E-002-015-ET, and 102-3113-P-002-026).

## REFERENCES

- (1) Geddes, C. D.; Lakowicz, J. R. Metal-Enhanced Fluorescence. *J. Fluoresc.* **2002**, *12*, 121–129.
- (2) Fort, E.; Gresillon, S. Surface Enhanced Fluorescence. *J. Phys. D: Appl. Phys.* **2008**, *41*, 013001.
- (3) Wokaun, A.; Lutz, H. P.; King, A. P.; Wild, U. P.; Ernst, R. R. Energy-Transfer in Surface Enhanced Luminescence. *J. Chem. Phys.* **1983**, *79*, 509–514.
- (4) Weiss, S. Fluorescence Spectroscopy of Single Biomolecules. *Science* **1999**, *283*, 1676–1683.
- (5) West, J. L.; Halas, N. J. Engineered Nanomaterials for Biophotonics Applications: Improving Sensing, Imaging, and Therapeutics. *Annu. Rev. Biomed. Eng.* **2003**, *5*, 285–292.
- (6) Resch-Genger, U.; Grabolle, M.; Cavaliere-Jaricot, S.; Nitschke, R.; Nann, T. Quantum Dots Versus Organic Dyes as Fluorescent Labels. *Nat. Methods* **2008**, *5*, 763–775.
- (7) Gu, X. F.; Qiu, T.; Zhang, W. J.; Chu, P. K. Light-Emitting Diodes Enhanced by Localized Surface Plasmon Resonance. *Nanoscale Res. Lett.* **2011**, *6*, 199.
- (8) Neogi, A.; Lee, C. W.; Everitt, H. O.; Kuroda, T.; Tackeuchi, A.; Yablonovitch, E. Enhancement of Spontaneous Recombination Rate in a Quantum Well by Resonant Surface Plasmon Coupling. *Phys. Rev. B* **2002**, *66*, 153305.
- (9) Vuckovic, J.; Loncar, M.; Scherer, A. Surface Plasmon Enhanced Light-Emitting Diode. *IEEE J. Quantum Electron.* **2000**, *36*, 1131–1144.
- (10) Gontijo, I.; Boroditsky, M.; Yablonovitch, E.; Keller, S.; Mishra, U. K.; DenBaars, S. P. Coupling of InGaN Quantum-Well Photoluminescence to Silver Surface Plasmons. *Phys. Rev. B* **1999**, *60*, 11564–11567.
- (11) Barnes, W. L. Electromagnetic Crystals for Surface Plasmon Polaritons and the Extraction of Light from Emissive Devices. *J. Lightwave Technol.* **1999**, *17*, 2170–2182.
- (12) Kock, A.; Gornik, E.; Hauser, M.; Beinstingl, W. Strongly Directional Emission from AlGaAs/GaAs Light-Emitting-Diodes. *Appl. Phys. Lett.* **1990**, *57*, 2327–2329.
- (13) Hecker, N. E.; Hopfel, R. A.; Sawaki, N.; Maier, T.; Strasser, G. Surface Plasmon-Enhanced Photoluminescence from a Single Quantum Well. *Appl. Phys. Lett.* **1999**, *75*, 1577–1579.
- (14) Hobson, P. A.; Wedge, S.; Wasey, J. A. E.; Sage, I.; Barnes, W. L. Surface Plasmon Mediated Emission from Organic Light-Emitting Diodes. *Adv. Mater.* **2002**, *14*, 1600–1600.
- (15) Okamoto, K.; Niki, I.; Shvartser, A.; Narukawa, Y.; Mukai, T.; Scherer, A. Surface-Plasmon-Enhanced Light Emitters Based on InGaN Quantum Wells. *Nat. Mater.* **2004**, *3*, 601–605.
- (16) Kulakovitch, O.; Strekal, N.; Yaroshevich, A.; Maskevich, S.; Gaponenko, S.; Nabiev, I.; Woggon, U.; Artemyev, M. Enhanced Luminescence of CdSe Quantum Dots on Gold Colloids. *Nano Lett.* **2002**, *2*, 1449–1452.
- (17) Liu, K. W.; Tang, Y. D.; Cong, C. X.; Sum, T. C.; Huan, A. C. H.; Shen, Z. X.; Wang, L.; Jiang, F. Y.; Sun, X. W.; Sun, H. D. Giant

- Enhancement of Top Emission from ZnO Thin Film by Nano-patterned Pt. *Appl. Phys. Lett.* **2009**, *94*, 151102.
- (18) Lin, Y.; Liu, X. Q.; Wang, T.; Chen, C.; Wu, H.; Liao, L.; Liu, C. Shape-Dependent Localized Surface Plasmon Enhanced UV-Emission from ZnO Grown by Atomic Layer Deposition. *Nanotechnology* **2013**, *24*, 125705.
- (19) Jeanmaire, D. L.; Van Duyne, R. P. Surface Raman Spectroelectrochemistry: Part I. Heterocyclic, Aromatic, and Aliphatic Amines Adsorbed on Anodized Silver Electrode. *J. Electroanal. Chem.* **1977**, *84*, 1–20.
- (20) Kneipp, K.; Wang, Y.; Kneipp, H.; Perelman, L. T.; Itzkan, I.; Dasari, R.; Feld, M. S. Single Molecule Detection Using Surface-Enhanced Raman Scattering (SERS). *Phys. Rev. Lett.* **1997**, *78*, 1667–1670.
- (21) Nie, S.; Emory, S. R. Probing Single Molecules and Single Nanoparticles by Surface-Enhanced Raman Scattering. *Science* **1997**, *275*, 1102–1106.
- (22) Moskovits, M. Surface-Enhanced Raman Spectroscopy: A Brief Retrospective. *J. Raman Spectrosc.* **2005**, *36*, 485–496.
- (23) Giannini, V.; Fernandez-Dominguez, A. I.; Heck, S. C.; Maier, S. A. Plasmonic Nanoantennas: Fundamentals and Their Use in Controlling the Radiative Properties of Nanoemitters. *Chem. Rev.* **2011**, *111*, 3888–3912.
- (24) Gaponenko, S. V. Plasmonic Enhancement of Spontaneous Emission and Scattering of Light in Nanostructures. *J. Optoelectron. Adv. Mater.* **2010**, *12*, 39–42.
- (25) Moskovits, M. Surface-Enhanced Spectroscopy. *Rev. Mod. Phys.* **1985**, *57*, 783–826.
- (26) Sun, G.; Khurgin, J. B. Origin of Giant Difference between Fluorescence, Resonance, and Nonresonance Raman Scattering Enhancement by Surface Plasmons. *Phys. Rev. A* **2012**, *85*, 063410.
- (27) Etchegoin, P. G.; Le Ru, E. C. Basic Electromagnetic Theory of SERS. In *Surface Enhanced Raman Spectroscopy: Analytical, Biophysical and Life Science Applications*; Schlucker, S., Kiefer, W., Eds.; Wiley-VCH: Weinheim, 2011; pp 1–37.
- (28) Petryayeva, E.; Krull, U. J. Localized Surface Plasmon Resonance: Nanostructures, Bioassays and Biosensing—a Review. *Anal. Chim. Acta* **2011**, *706*, 8–24.
- (29) Le Ru, E. C.; Etchegoin, P. G. *Principles of Surface-Enhanced Raman Spectroscopy: and Related Plasmonic Effects*; Elsevier Science: London, 2009.
- (30) Khurgin, J. B.; Sun, G. Enhancement of Optical Properties of Nanoscaled Objects by Metal Nanoparticles. *J. Opt. Soc. Am. B* **2009**, *26*, B83–B95.
- (31) Sun, G.; Khurgin, J. B.; Yang, C. C. Impact of High-Order Surface Plasmon Modes of Metal Nanoparticles on Enhancement of Optical Emission. *Appl. Phys. Lett.* **2009**, *95*, 171103.
- (32) Ozgur, U.; Alivov, Y. I.; Liu, C.; Teke, A.; Reschchikov, M. A.; Dogan, S.; Avrutin, V.; Cho, S. J.; Morkoc, H. A Comprehensive Review of ZnO Materials and Devices. *J. Appl. Phys.* **2005**, *98*, 041301.
- (33) Langhammer, C.; Yuan, Z.; Zoric, I.; Kasemo, B. Plasmonic Properties of Supported Pt and Pd Nanostructures. *Nano Lett.* **2006**, *6*, 833–838.
- (34) Suzuki, T.; Miyata, H.; Noma, T.; Kuroda, K. Platinum Thin Film Consisting of Well-Aligned Nanowires and Its Optical Behavior. *J. Phys. Chem. C* **2008**, *112*, 1831–1836.
- (35) Joo, S. H.; Choi, S. J.; Oh, I.; Kwak, J.; Liu, Z.; Terasaki, O.; Ryoo, R. Ordered Nanoporous Arrays of Carbon Supporting High Dispersions of Platinum Nanoparticles. *Nature* **2001**, *412*, 169–172.
- (36) Peng, Z. M.; You, H. J.; Wu, J. B.; Yang, H. Electrochemical Synthesis and Catalytic Property of Sub-10 nm Platinum Cubic Nanoboxes. *Nano Lett.* **2010**, *10*, 1492–1496.
- (37) Sun, Y. G.; Xia, Y. N. Shape-Controlled Synthesis of Gold and Silver Nanoparticles. *Science* **2002**, *298*, 2176–2179.
- (38) Rycenga, M.; Cobley, C. M.; Zeng, J.; Li, W. Y.; Moran, C. H.; Zhang, Q.; Qin, D.; Xia, Y. N. Controlling the Synthesis and Assembly of Silver Nanostructures for Plasmonic Applications. *Chem. Rev.* **2011**, *111*, 3669–3712.
- (39) Wiley, B.; Sun, Y. G.; Mayers, B.; Xia, Y. N. Shape-Controlled Synthesis of Metal Nanostructures: The Case of Silver. *Chem.—Eur. J.* **2005**, *11*, 454–463.
- (40) Tseng, A. A. Recent Developments in Nanofabrication Using Focused Ion Beams. *Small* **2005**, *1*, 924–939.
- (41) Hicks, E. M.; Zou, S. L.; Schatz, G. C.; Spears, K. G.; Van Duyne, R. P.; Gunnarsson, L.; Rindzevicius, T.; Kasemo, B.; Kall, M. Controlling Plasmon Line Shapes through Diffractive Coupling in Linear Arrays of Cylindrical Nanoparticles Fabricated by Electron Beam Lithography. *Nano Lett.* **2005**, *5*, 1065–1070.
- (42) Shevchenko, A.; Ovchinnikov, V.; Shevchenko, A. Large-Area Nanostructured Substrates for Surface Enhanced Raman Spectroscopy. *Appl. Phys. Lett.* **2012**, *100*, 171913.
- (43) Ritala, M.; Leskela, M. Atomic Layer Epitaxy - a Valuable Tool for Nanotechnology? *Nanotechnology* **1999**, *10*, 19–24.
- (44) Kim, H.; Lee, H. B. R.; Maeng, W. J. Applications of Atomic Layer Deposition to Nanofabrication and Emerging Nanodevices. *Thin Solid Films* **2009**, *517*, 2563–2580.
- (45) George, S. M. Atomic Layer Deposition: An Overview. *Chem. Rev.* **2010**, *110*, 111–131.
- (46) Profijt, H. B.; Potts, S. E.; van de Sanden, M. C. M.; Kessels, W. M. M. Plasma-Assisted Atomic Layer Deposition: Basics, Opportunities, and Challenges. *J. Vac. Sci. Technol., A* **2011**, *29*, 050801.
- (47) Im, H.; Wittenberg, N. J.; Lindquist, N. C.; Oh, S. H. Atomic Layer Deposition: A Versatile Technique for Plasmonics and Nanobiotechnology. *J. Mater. Res.* **2012**, *27*, 663–671.
- (48) Frohlich, K.; Tapajna, M.; Rosova, A.; Dobrocka, E.; Husekova, K.; Aarik, J.; Aidla, A. Growth of High-Dielectric-Constant TiO<sub>2</sub> Films in Capacitors with RuO<sub>2</sub> Electrodes. *Electrochem. Solid-State Lett.* **2008**, *11*, G19–G21.
- (49) Xia, Y. N.; Halas, N. J. Shape-Controlled Synthesis and Surface Plasmonic Properties of Metallic Nanostructures. *MRS Bull.* **2005**, *30*, 338–344.
- (50) Willets, K. A.; Van Duyne, R. P. Localized Surface Plasmon Resonance Spectroscopy and Sensing. *Annu. Rev. Phys. Chem.* **2007**, *58*, 267–297.
- (51) Lin, M. C.; Nien, L. W.; Chen, C. H.; Lee, C. W.; Chen, M. J. Surface Enhanced Raman Scattering and Localized Surface Plasmon Resonance of Nanoscale Ultrathin Films Prepared by Atomic Layer Deposition. *Appl. Phys. Lett.* **2012**, *101*, 023112.
- (52) Baker, L.; Cavanagh, A. S.; Seghete, D.; George, S. M.; Mackus, A. J. M.; Kessels, W. M. M.; Liu, Z. Y.; Wagner, F. T. Nucleation and Growth of Pt Atomic Layer Deposition on Al<sub>2</sub>O<sub>3</sub> Substrates Using (Methylcyclopentadienyl)-Trimethyl Platinum and O<sub>2</sub> Plasma. *J. Appl. Phys.* **2011**, *109*, 084333.
- (53) Novak, S.; Lee, B.; Yang, X. Y.; Misra, V. Platinum Nanoparticles Grown by Atomic Layer Deposition for Charge Storage Memory Applications. *J. Electrochem. Soc.* **2010**, *157*, H589–H592.
- (54) Aaltonen, T.; Ritala, M.; Sajavaara, T.; Keinonen, J.; Leskela, M. Atomic Layer Deposition of Platinum Thin Films. *Chem. Mater.* **2003**, *15*, 1924–1928.
- (55) Kelly, K. L.; Coronado, E.; Zhao, L. L.; Schatz, G. C. The Optical Properties of Metal Nanoparticles: The Influence of Size, Shape, and Dielectric Environment. *J. Phys. Chem. B* **2003**, *107*, 668–677.
- (56) Miller, M. M.; Lazarides, A. A. Sensitivity of Metal Nanoparticle Surface Plasmon Resonance to the Dielectric Environment. *J. Phys. Chem. B* **2005**, *109*, 21556–21565.
- (57) Maier, S. A. Plasmonic Field Enhancement and SERS in the Effective Mode Volume Picture. *Opt. Express* **2006**, *14*, 1957–1964.
- (58) Fox, M. *Optical Properties of Solids*. 2nd ed.; Oxford University Press: New York, 2010.
- (59) Baer, W. S. Faraday Rotation in ZnO - Determination of Electron Effective Mass. *Phys. Rev.* **1967**, *154*, 785–789.
- (60) Beni, G.; Rice, T. M. Theory of Electron-Hole Liquid in Semiconductors. *Phys. Rev. B* **1978**, *18*, 768–785.
- (61) Fan, W. J.; Xia, J. B.; Agus, P. A.; Tan, S. T.; Yu, S. F.; Sun, X. W. Band Parameters and Electronic Structures of Wurtzite ZnO and ZnO/MgZnO Quantum Wells. *J. Appl. Phys.* **2006**, *99*, 013702.

- (62) Makino, T.; Chia, C. H.; Tuan, N. T.; Sun, H. D.; Segawa, Y.; Kawasaki, M.; Ohtomo, A.; Tamura, K.; Koinuma, H. Room-Temperature Luminescence of Excitons in ZnO/(Mg, Zn)O Multiple Quantum Wells on Lattice-Matched Substrates. *Appl. Phys. Lett.* **2000**, *77*, 975–977.
- (63) Sze, S. M. *Physics of Semiconductor Devices*; Wiley-Interscience: Hoboken, NJ, 2007.
- (64) Zhang, X.; Zhao, J.; Whitney, A. V.; Elam, J. W.; Van Duyne, R. P. Ultrastable Substrates for Surface-Enhanced Raman Spectroscopy: Al<sub>2</sub>O<sub>3</sub> Overlays Fabricated by Atomic Layer Deposition Yield Improved Anthrax Biomarker Detection. *J. Am. Chem. Soc.* **2006**, *128*, 10304–10309.
- (65) Im, H.; Lindquist, N. C.; Lesuffleur, A.; Oh, S. H. Atomic Layer Deposition of Dielectric Overlays for Enhancing the Optical Properties and Chemical Stability of Plasmonic Nanoholes. *ACS Nano* **2010**, *4*, 947–954.
- (66) Barrios, C. A.; Malkovskiy, A. V.; Kisliuk, A. M.; Sokolov, A. P.; Foster, M. D. Highly Stable, Protected Plasmonic Nanostructures for Tip Enhanced Raman Spectroscopy. *J. Phys. Chem. C* **2009**, *113*, 8158–8161.
- (67) Christensen, S. T.; Elam, J. W.; Rabuffetti, F. A.; Ma, Q.; Weigand, S. J.; Lee, B.; Seifert, S.; Stair, P. C.; Poeppelmeier, K. R.; Hersam, M. C.; et al. Controlled Growth of Platinum Nanoparticles on Strontium Titanate Nanocubes by Atomic Layer Deposition. *Small* **2009**, *5*, 750–757.
- (68) Jiang, X. R.; Huang, H.; Prinz, F. B.; Bent, S. F. Application of Atomic Layer Deposition of Platinum to Solid Oxide Fuel Cells. *Chem. Mater.* **2008**, *20*, 3897–3905.